IEEE Photonics Journal
An IEEE Photonics Society Publication

High Performance Polarization Beam Splitter Based on Cascaded Directional Couplers Assisted by Effectively Anisotropic Structures

Volume 11, Number 6, December 2019

Kaixuan Chen
Kyoungsik Yu
Sailing He, ***Fellow, IEEE***

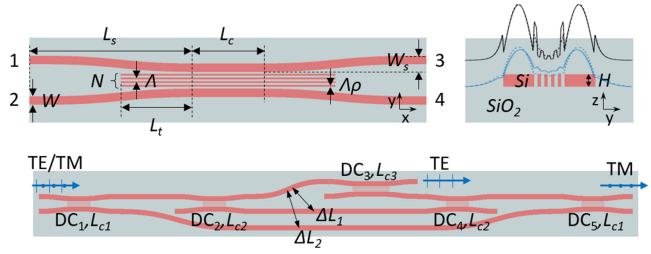

DOI: 10.1109/JPHOT.2019.2950065

High Performance Polarization Beam Splitter Based on Cascaded Directional Couplers Assisted by Effectively Anisotropic Structures

Kaixuan Chen,[1,2] Kyoungsik Yu,[2] and Sailing He,[1] *Fellow, IEEE*

[1]Center for Optical and Electromagnetic Research, National Engineering Research Center for Optical Instruments, Zhejiang University, Hangzhou 310058, China
[2]School of Electrical Engineering, Korea Advanced Institute of Science and Technology, Daejeon 34141, South Korea

DOI:10.1109/JPHOT.2019.2950065

Manuscript received August 17, 2019; revised October 12, 2019; accepted October 24, 2019. Date of publication October 28, 2019; date of current version December 13, 2019. This work was supported in part by The National Key Research and Development Program of China under Grant 2017YFA0205700, in part by the National Natural Science Foundation of China (NSFC) under Grant 11621101, and in part by the Institute for Information & communications Technology Promotion (IITP) Grant through by the Korea government (MSIT) under Grant 2019-0-01349, High-accuracy miniaturized optical frequency synthesizer for reliable quantum sensors. The work of K. Chen was supported by the China Scholarship Council (for 1-year study abroad at the Korea Advanced Institute of Science and Technology). Corresponding author: Sailing He (e-mail: sailing@zju.edu.cn).

Abstract: A high performance polarization beam splitter (PBS) based on cascaded directional couplers (DCs) assisted by effectively anisotropic structures is proposed. The sub-wavelength grating (SWG) structures between the two coupled waveguides act as anisotropic metamaterial cladding to block/enhance light coupling for transverse electric (TE)/magnetic (TM) polarization. Cascading the DCs designed at different central wavelengths can improve the extinction ratio (ER) within the desired bandwidth or broaden the working wavelength bandwidth for TM polarization. Three design examples show the excellent performance of PBS with ER of $>$35 dB, 20 dB or 14 dB and loss of $<$0.12 dB, 0.4 dB or 0.8 dB over a bandwidth (BW) of 60 nm, 250 nm or 400 nm, which is difficult to achieve in any PBS structure reported before. The $BW_{ER>20dB}$ of the PBS based on the cascaded DCs increases by $\sim$11 times when compared with a single DC.

Index Terms: Polarization beam splitter, sub-wavelength grating, anisotropic metamaterial.

1. Introduction

On-chip polarization beam splitters (PBSs) have been widely used in polarization management devices on high index contrast platform, such as the polarization-division multiplexing systems on silicon-on-insulator (SOI), where optical signals with different polarizations can be separated/combined from/into one single waveguide [1], [2]. Various silicon-based on-chip PBSs have been demonstrated by employing different structures, such as multi-mode interference (MMI) couplers [3], Mach–Zehnder interferometers (MZIs) [4], grating-assisted contra-directional couplers [5] and directional couplers (DCs) [6]–[14]. Among them, the asymmetric DCs provide competitive solutions due to the compact size and high extinction ratio (ER). Most DC-based PBSs introduce significant phase mismatch for transverse electric (TE) polarization within the DC while keeping

the phase matching condition for transverse magnetic (TM) polarization [8]–[14]. Thus, the TE polarization can propagate through the same input waveguide throughout the DC while TM polarization will couple into another waveguide. The working bandwidth of this PBS strategy is usually limited by the TM polarization since it shows much more dispersion than the TE polarization case in the coupled waveguide system [8]–[12]. The improvement for the ER and bandwidth has been proposed by cascading two DCs for two-stage polarization filtering [6], [9]–[11]. A remarkable PBS performance has been demonstrated in [10] with ER $>$20 dB and estimated insertion loss of $<$1 dB over $\sim$135 nm bandwidth. In such a cascaded strategy, the central wavelengths of two DCs are only slightly different or the same. The second-stage DC cannot be used to filter the large residual light at the wavelength deviated far from the central wavelength, where it suffers high optical losses. Thus, the bandwidth of the reported PBS using cascaded DCs is also limited. In [14], the bandwidth of ER $>$20 dB was improved to $\sim$175 nm based on a DC consisting of a shallow taper-etched waveguide and a slot waveguide. Unfortunately, it still suffered high optical losses in the long wavelength region and needed additional etching processes for two-step waveguides. Sub-wavelength grating (SWG) structures have been used to control the dispersions to enhance the operation bandwidth in couplers [15]–[17]. The engineering on anisotropy of the SWGs can enlarge the difference between the beat lengths for TE and TM polarization, therefore a shorter and broadband PBS also can be achieved [18]–[20]. An ultra-compact PBS using SWG-based anisotropic metamaterials shows a record working bandwidth $>$200 nm with a small loss of $<$1 dB and a large ER of $>$20 dB [21].

In addition to constructing phase mismatch structure in a DC to prevent the light coupling, sub-wavelength-scale structures have been added as anisotropic metamaterial side-cladding to suppress evanescent waves for one polarization, which results in low coupling between waveguides, while it does not work for its orthometric polarization [22], [23]. Inspired by these effects, a single symmetric DC assisted by an SWG can be implemented to separate two polarization signals. The SWG between two coupled waveguides acts as anisotropic metamaterial side-cladding to suppress TE evanescent waves while enhance the TM coupling. Thus, the coupling length of TE/TM mode will further increase/decrease compared to the normal DC without SWG. In this paper, we take advantage of the SWG-based anisotropic metamaterial to separate the TE polarization in DCs and greatly improve the TM coupling performance via novel cascaded DCs. Different from aforementioned methods, our cascaded strategy allows the TE polarized light to pass through fewer DCs.

2. Basic Structure and Principle

2.1 Directional Coupler Assisted by Sub-Wavelength Grating

The proposed basic DC structure consists of a normal DC and an SWG mediating between the two coupled waveguides on a 220-nm-thick SOI platform with silicon dioxide upper-cladding, as shown in Figs. 1(a) and 1(b). The overall DC structure is divided into two S-bend input/output sections and a straight coupling region. The length of the SWG is slightly longer than that of straight coupling region because the S-bend parts can also introduce some coupling. When TE and TM light waves input from port 1, TE light will pass through port 3 while TM light couples into port 4 at the designed central wavelength. Here is the working principle. The total internal reflection (TIR) condition at the interface of an isotropic and an anisotropic dielectric is relaxed to $n_{Si} > \sqrt{\varepsilon_y}$, where n_{Si} is the refractive index of core medium silicon and ε_y is the dielectric constant of anisotropic cladding medium along the direction perpendicular to the interface [23], [24]. An anisotropic dielectric metamaterial can be made by an SWG structure when the grating period is much smaller than the wavelength of the light [15], [23]. The relaxed-TIR realized by an SWG anisotropic metamaterial cladding provides a new degree of freedom, the component ε_x of the dielectric tensor parallel to the interface, to control the momentum in the perpendicular direction, i.e., evanescent waves in the side cladding [23]. The decay constants of the evanescent wave in the SWG anisotropic metamaterial cladding can be

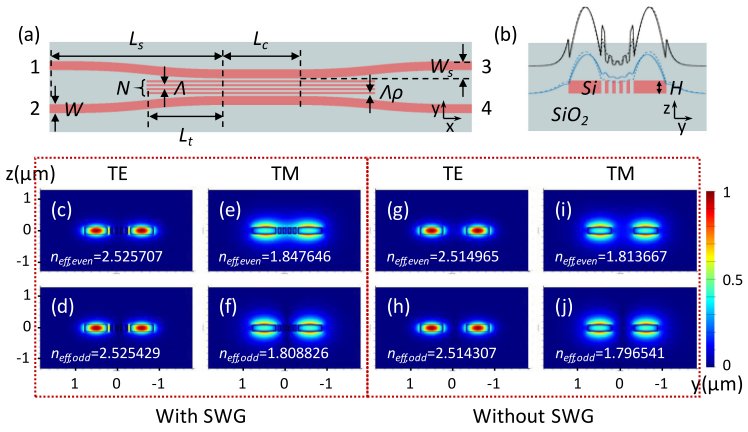

Fig. 1. (a) The proposed DC assisted by SWG for the PBS purpose. (b) The cross section in the straight coupling region. The inserted profiles are for the amplitude of E_x fields of its fundamental TE modes (black) and the amplitude of E_y fields of its fundamental TM modes (blue), with (solid lines) and without (dotted lines) the SWG between the coupled waveguides. Amplitude distributions of the electric field of the even and odd modes for TE and TM polarizations in the coupled waveguides with (c)–(f) and without (g)–(j) the SWG structure.

obtained from the dispersion relation of TE/TM polarized waves [24], [25], which are given by

$$\text{TE}: \frac{(k_x)^2}{\varepsilon_y} + \frac{(k_y)^2}{\varepsilon_x} = (k_0)^2 \rightarrow k_y = \sqrt{\frac{\varepsilon_x}{\varepsilon_y}}\sqrt{\varepsilon_x(k_0)^2 - (k_x)^2}, \tag{1}$$

$$\text{TM}: \frac{(k_x)^2}{\varepsilon_z} + \frac{(k_y)^2}{\varepsilon_x} = (k_0)^2 \rightarrow k_y = \sqrt{\varepsilon_x(k_0)^2 - (k_x)^2}, \tag{2}$$

where k_0 is the wave vector in free space and k_x is the parallel components of the wave vector in the SWG anisotropic metamaterial cladding. For a quasi-2D strip waveguide model, we have $\varepsilon_z = \varepsilon_x$. The decay rate of TE evanescent waves can be enhanced by increasing the ratio of $\sqrt{\varepsilon_x/\varepsilon_y}$. By controlling periodicity Λ and silicon duty cycle ρ of the SWG, the largest decay constant can be achieved near $\rho = 0.5$, which means evanescent wave will be more strongly confined close to the interface for TE polarization. For TM polarization, the increased ε_x will always alleviate the decay rate. Thus, the TM coupling in the proposed DC will be stronger than that without the SWG. In the proposed structure, for easy fabrication we chose width of the waveguides $W = 0.55$ μm, period number $N = 4$, $\Lambda = 120$ nm far less than the operation wavelength and $\rho = 0.5$ with the ratio of $\sqrt{\varepsilon_x/\varepsilon_y}$ about 1.41 at the wavelength of 1550 nm. The anisotropy properties in the SWG are obtained by $\varepsilon_z = \varepsilon_x = \varepsilon_{Si}\rho + \varepsilon_{SiO_2}(1-\rho)$ and $1/\varepsilon_y = \rho/\varepsilon_{Si} + (1-\rho)/\varepsilon_{SiO_2}$ [15]. The electric field profiles of the fundamental mode at the center of the cross section in the straight coupling region are inserted in Fig. 1(b). One can see that more evanescent wave of the TE polarization (black curves) concentrates near the waveguides with the SWG structure compared to that without SWG, while it is the other way around for the TM polarization (blue curves).

The advantage of DC assisted by the SWG for PBS can be further quantitatively analyzed by calculating their beat length (or coupling length) L_π. Figs. 1(c)–1(j) show the cross-sectional electric field distributions of the even and odd supermodes in the straight coupled waveguide region with/without the SWG and their corresponding effective indices n_{eff}. The mode profiles are calculated by the finite-element method (Lumerical MODE Solutions). As predicted earlier, more evanescent power of TE polarization in the SWG structure concentrates near the waveguide side surfaces than the case without the SWG, while it is opposite for the TM polarization. It is noted that the effective index difference between the even and odd modes originates from their symmetric/antisymmetric properties: the field intensity of the odd mode is zero at the center of the coupled waveguides while it is not for the even mode. The introduced SWG will alleviate/aggravate these differences

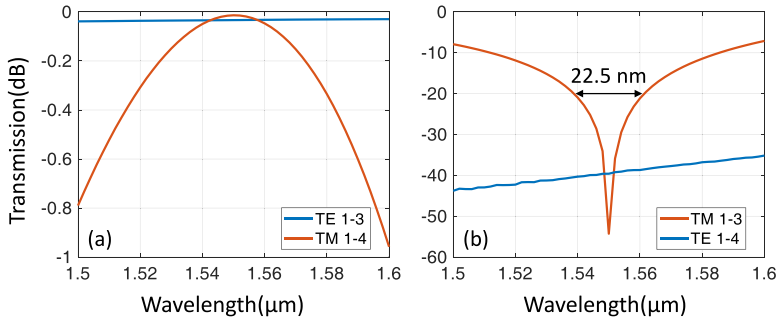

Fig. 2. Wavelength responses in a single DC assisted by an SWG structure.

for TE/TM polarization, which results in some reduction/increase in the effective index difference between even and odd modes. Coupling length L_π for TE/TM polarization is then calculated as 2787.77 μm/19.96 μm at 1.55 μm wavelength, which is larger/smaller than 1177.81 μm/45.25 μm in the DC without the SWG. L_π of these modes is obtained by $L_\pi = \lambda/(n_{eff,even} - n_{eff,odd})/2$, where λ, $n_{eff,even}$ and $n_{eff,odd}$ are the wavelength, effective indices of even and odd modes, respectively. Considering the coupling in the S-bend input/output sections, the parameters of the S bend waveguides are fixed with $W_s = 1.05$ μm and $L_s = 15$ μm for low bending loss over ultra-broadband designed below. Length L_t of the SWG section in the S-bend region is 5 μm. Based on the weakly coupled mode theory [26], [27], the coupled equations can be formed as

$$\frac{d}{dx}\begin{bmatrix} A_1(x) \\ A_2(x) \end{bmatrix} = i\begin{bmatrix} \beta_0 + \delta(x) & k(x) \\ k(x) & \beta_0 + \delta(x) \end{bmatrix}\begin{bmatrix} A_1(x) \\ A_2(x) \end{bmatrix}, \tag{3}$$

where $A_1(x)$ and $A_2(x)$ are the amplitudes in two single mode waveguides at x position, β_0 is the propagation constant of an uncoupled waveguide mode, $\delta(x)$ is the correction parameter and $k(x)$ is the coupling constant. All of them are wavelength dependent and can be extracted from the effective refractive indices of the waveguide modes:

$$\beta_0 = k_0 n_{eff,wg}, \tag{4}$$

$$\delta(x) = \frac{k_0}{2}\left[n_{eff,even}(x) + n_{neff,odd}(x) - 2n_{eff,wg}\right], \tag{5}$$

$$k(x) = \frac{k_0}{2}\left[n_{eff,even}(x) - n_{neff,odd}(x)\right], \tag{6}$$

where $n_{eff,wg}$, $n_{eff,even}$, $n_{eff,odd}$ are the effective indices of an uncoupled waveguide mode, even and odd modes in the coupled waveguides, respectively. The calculated transmissions of the proposed DC are shown in Fig. 2 with the length of straight coupling length $L_c = 11.6$ μm at the central wavelength of 1.55 μm. The legend of 'TM 1-4', for example, denotes the TM transmission from port 1 to port 4. One can find that the PBS performances for TE polarizations (blue curves) are excellent with an optical loss $<$0.04 dB and ER $>$35 dB over the 100 nm bandwidth. For TM polarizations, however, we can obtain low loss and high ER only near the central wavelength, and the bandwidth of ER $>$20 dB, labeled as $BW_{ER>20\,dB}$, is limited to 22.5 nm. One should be noted that although the effective anisotropy in the SWG structures is similar to that in anisotropy-engineered PBS reported before [4], [24], [33], [34], the high performance for TE polarization in our structure benefits from the relaxed-TIR mechanism. And the evanescent waves control based on relaxed-TIR is quite different from the slot waveguides, which utilize nanoscale field enhancement.

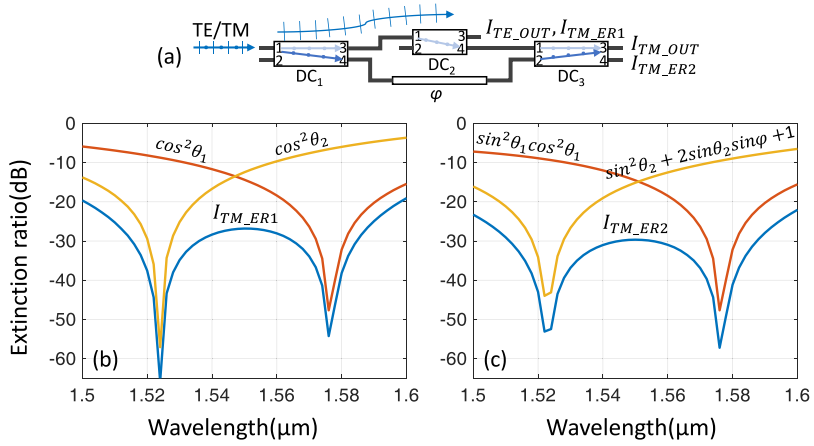

Fig. 3. The principle of the proposed high-performance PBS with cascaded DCs. (a) Basic cascaded structure and the TE/TM light transmission route. (b) The remaining TM part output from port 3 in DC_1 can be further suppressed by DC_2. (c) The TM light coming out from port 4 of DC_1 and DC_2 will be combined into port 3 of DC_3 with the phase shifter.

2.2 Cascaded Directional Couplers for Broadening the Optical Bandwidth

Such anisotropic-metamaterial-assisted DC has highly predictable high ER and broadband for the TE polarization. However, its overall performance is limited to the bandwidth of the TM polarization due to the natural dispersion in the coupled system. Now the challenge is how to increase the TM coupling bandwidth. Traditional methods to improve the working bandwidth in a single DC, such as bending [28], adiabatic [29] and asymmetric [30] structures, become difficult especially beyond 100 nm bandwidth or hard to achieve 100% coupling. The wavelength insensitivity of couplers can be realized from two cascaded DCs with an intermediate phase delay [31]. The bandwidth of silicon optical switches based on such cascaded DCs can be $>$100 nm [32], [33]. Optical silicon switches were designed for a large bandwidth of $>$250 nm by using four cascaded Mach-Zehnder interferometers (MZIs) [34]. This idea of offsetting the wavelength sensitivity by multiple DCs provides a great potential to broaden the TM bandwidth in a PBS, where TE polarization can pass through all DCs straightly without coupling and only TM polarization needs to be considered. However, if their structure is used for PBS function, TE-polarized light has to suffer a long optical path when there are too many cascaded DCs, which will deteriorate the ER and loss for TE polarization.

A novel cascaded DCs strategy is proposed here to increase the TM coupling bandwidth without deteriorating the TE performance. To illustrate the principle, only the straight coupling region is considered and the transmission in a single DC shown in Fig. 1(a) can be expressed by a transfer matrix:

$$\begin{bmatrix} E_3 \\ E_4 \end{bmatrix} = \begin{bmatrix} \cos\theta & j\sin\theta \\ j\sin\theta & \cos\theta \end{bmatrix} \begin{bmatrix} E_1 \\ E_2 \end{bmatrix}, \tag{7}$$

where E_1 and E_2 are the input amplitudes from ports 1 and 2, E_3 and E_4 are the output amplitudes from ports 3 and 4, and $\theta = kL_c$. The simplest cascaded-DCs we proposed is shown in Fig. 3(a), which consists of three DCs and a phase shifter. DC_1 and DC_2 have different coupling lengths, which correspond to different center wavelengths λ_1 and λ_2 respectively for the TM polarization. DC_3 has the same structure as DC_1. When TE and TM polarization waves input from port 1 in DC_1, TE polarization power will go through port 3 in DC_1 and DC_2 directly (denoted by I_{TE_OUT}), while almost all of the TM polarization at wavelength λ_1 and some of them at wavelength λ_2 will be coupled into port 4 in DC_1 and the remaining part at wavelength λ_2 will be coupled into port 4 in DC_2. After the phase control for two inputs, DC_3 acts as a combiner and TM polarization power will be output from port 3 in DC_3 (denoted by I_{TM_OUT}). We consider the TM power portions come out

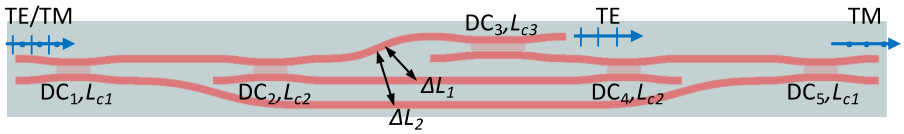

Fig. 4. The proposed PBS with five cascaded DCs. All the DCs assisted by the SWG structures have the same parameters except the coupling lengths.

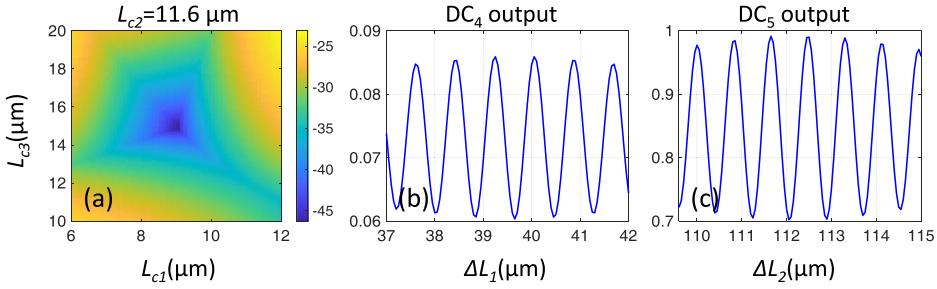

Fig. 5. Optimization for TM transmission by scanning (a) coupling lengths L_{c1}, L_{c2} and L_{c3}, (b) length difference ΔL_1, and (c) length difference ΔL_2.

from port 3 in DC_2 (denoted by I_{TM_ER1}) and port 4 in DC_3 (denoted by I_{TM_ER2}) according to Eq. (7):

$$I_{TM\_ER1} = \cos^2\theta_1 \cos^2\theta_2, \tag{8}$$

$$I_{TM\_ER2} = \sin^2\theta_1 \cos^2\theta_1 \left(\sin^2\theta_2 + 2\sin\theta_2 \sin\varphi + 1\right), \tag{9}$$

where θ_1 and θ_2 are the angular expressions of the amplitude coupling ratios of DC_1 and DC_2, respectively, and φ is the shifted phase between port 4 in DC_1 and port 2 in DC_3. Actually, I_{TM_ER1} is the product of DC_1 and DC_2 responses. Due to their different central wavelengths, the response of I_{TM_ER1} can be suppressed over broader bandwidth obviously, as shown in Fig. 3(b). In I_{TM_ER2}, the response of the first two items $\sin^2\theta_1\cos^2\theta_1$ is determined by DC_1 and its sidelobes can also be suppressed by the third item, as shown in Fig. 3(c). In a practical design, θ_1 and θ_2 can be chosen according to ER I_{TM_ER1} and its bandwidth for the TM polarization, and φ is then optimized to minimize I_{TM_ER2}, i.e., minimize the loss of TM output I_{TM_OUT}.

3. High Performance Polarization Beam Splitter Design

We extend the cascaded idea to five DCs, as shown in Fig. 4. TE polarization will come through port 3 in DC_1, DC_2 and DC_3, while TM polarization at different wavelength will be coupled into their port 4 and finally combined by DC_4 and DC_5. DC_4 and DC_5 have the same structure as DC_2 and DC_1, respectively. This designed example is aimed at high ER PBS over 60 nm bandwidth. The following transmission calculations are based on Eq. (3). Firstly, the coupling lengths of different DCs are designed to achieve high ER over 60 nm bandwidth. We fix the parameters of the input/output S-bend regions as above and calculate the TM transmission from port 4 by scanning L_c in a single DC. The scan range can be chosen around L_π at the wavelength evenly distributed within the design range of 1520–1580 nm, e.g., 1525 nm, 1550 nm and 1575 nm. The normalized TM transmission from port 4 of three DCs with different coupling lengths are then multiplied to find out the highest ER. The minimum TM transmission values in the range of 1520–1580 nm are compared with different L_{c1} and L_{c3} when L_{c2} is equal to L_π at the wavelength of 1550 nm, as shown in Fig. 5(a). L_{c1}, L_{c2} and L_{c3} are finally optimized to 9 μm, 11.6 μm, 14.8 μm with the minimum TM transmission, i.e., ER $>$47 dB over 60 nm bandwidth. The second step is to optimize optical path difference ΔL_1 of two arms between DC_2 and DC_4. The path difference doesn't include the DC_3 because the phase change in this section is calculated by its transfer matrix. The average TM transmission

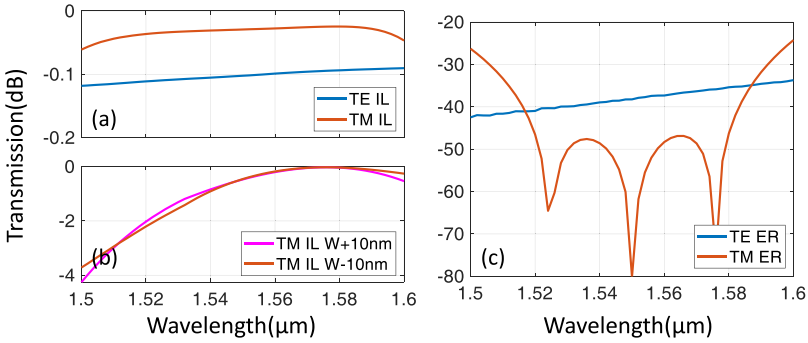

Fig. 6. Performances for the high ER PBS over 60 nm band: (a) IL and (c) ER for TE and TM polarization inputs and (b) IL for TM polarization inputs when the waveguide width of the phase shifter is varied by ±10 nm.

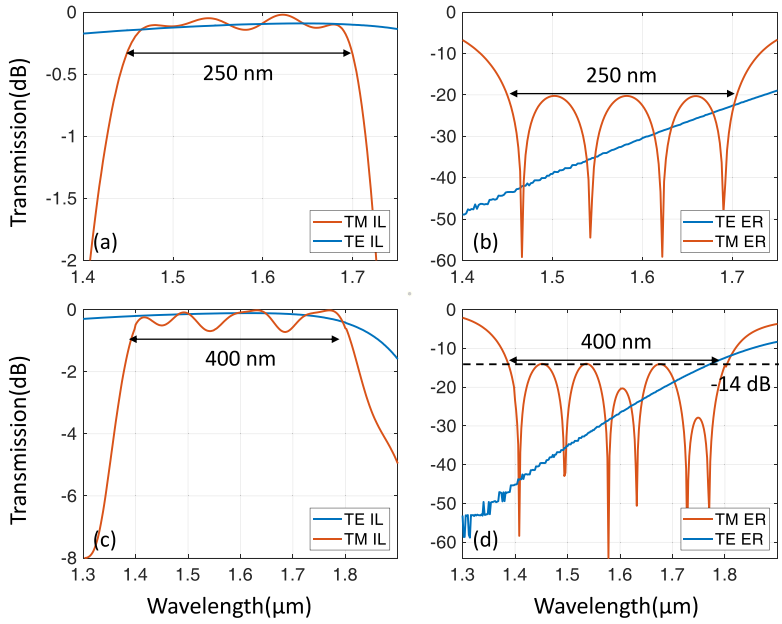

Fig. 7. (a)–(b) The PBS designs for ER >20 dB over 250 nm bandwidth with the parameters of $L_{c1} = 5.5\ \mu$m, $L_{c2} = 12.5\ \mu$m, $L_{c3} = 25.4\ \mu$m, $\Delta L_1 = 49.2\ \mu$m and $\Delta L_2 = 123.43\ \mu$m. (c)–(d) The ultra-broadband 400 nm designs with the parameters of $L_{c1} = 4.9\ \mu$m, $L_{c2} = 19.5\ \mu$m, $L_{c3} = 43.6\ \mu$m, $\Delta L_1 = 66.18\ \mu$m and $\Delta L_2 = 155.35\ \mu$m.

over 60 nm band from port 3 in DC_4 is calculated by scanning ΔL_1. One can find its maximal TM transmission in Fig. 5(b) with $\Delta L_1 = 39.24\ \mu$m. The sine oscillation of the curve is due to the multiple 2π phase shift and the envelope ascribes to the dispersion of the waveguide. Thus, the TM polarization output cannot be 100% for all wavelengths but with acceptable loss. The third step is similar to the second one: optimize the path difference ΔL_2 of two arms between DC_1 and DC_5. The path difference is also considered only by the length difference of the additional waveguides connecting between the DCs. The average power output from port 3 in DC_5 over 60 nm band is calculated by scanning ΔL_2, as shown in Fig. 5(c). ΔL_2 is chosen with 112.48 μm for the lowest loss. Finally, the TM and TE transmission output from ports 3 in DC_3 and DC_5 are verified in the whole cascaded DC structure, as shown in Figs. 6(a) and 6(c). The loss of <0.12 dB/0.04 dB and ER of >35 dB/45 dB over the wavelength range of 1520–1580 nm for TE/TM input can be achieved. In the practical implementation, the fabrication error of waveguide might introduce some

phase errors in waveguides, which can result in higher insertion loss for the TM mode output. As shown in Fig. 6(b), the maximum loss becomes 2 dB when a waveguide width variation of $\pm$10 nm is introduced for the phase shifter and other parameters of the PBS are fixed. Active phase shifters or thermal electrodes can be considered for more accurate phase control.

The working bandwidth can be further improved by relaxing ER. Using a design method similar to the above, the coupling lengths and phase compensations of the five cascaded DCs in Fig. 4 can be optimized to ultra-broadband 250 nm/400 nm with the ER of $>$20 dB/14 dB and loss $<$0.4 dB/0.8 dB for both TE and TM polarizations. These two sets of design are given by L_{c1} = 5.5 μm/4.9 μm, L_{c2} = 12.5 μm/19.5 μm, L_{c3} = 25.4 μm/43.6 μm, ΔL_1 = 49.2 μm/66.18 μm and ΔL_2 = 123.43 μm/155.35 μm. Their wavelength responses are shown in Fig. 7. The calculations using Eq. (3) match well with finite-different time-domain method (Lumerical FDTD Solutions) in single DCs with different coupling lengths. In the ultra-broadband designs, there are some fluctuations in the TM responses due to the dispersion of the phase shifter, the same reason as seen in the envelope oscillation in Figs. 5(b) and 5(c) when varying the waveguide length of the phase shifter. Although it is difficult to have 100% TM polarization output for some wavelengths, the losses can be kept low over the ultra-broad band wavelength range.

4. Conclusion

By taking advantage of the anisotropic SWG structures for polarization-dependent evanescent wave control, the TE polarization can be selectively separated in the proposed DC structures. The ER and bandwidth of the TM polarization response are significantly improved by employing the cascaded design strategy. Three design examples have been given to show the excellent performance of PBS with ER of $>$35 dB, 20 dB or 14 dB and loss of $<$0.12 dB, 0.4 dB or 0.8 dB over the bandwidth of 60 nm, 250 nm or 400 nm, which is difficult to achieve in any PBS structure reported before. The $BW_{ER>20dB}$ of the proposed PBS has been increased by $\sim$11 times when compared with a single DC. One can also use three or more cascaded DCs to improve the PBS performance by trading off the overall footprint. We believe that the performance of any PBS with a coupling mechanism of TE-through and TM-cross, whose performance is mainly limited by TM polarization [8]–[12], [21], can be further improved by using our cascaded structure demonstrated in this paper. Moreover, higher-performance DCs can reduce the number of the cascaded DCs required and achieve more compact size. A smaller footprint design and improvement of the tolerance to fabrication inaccuracies for the full metastructures with better performance and robustness can be considered by using the inverse design method [35], [36], particularly the deep learning methods demonstrated in nanophotonic design recently [37], [38].

References

[1] P. Dong, "Silicon photonic integrated circuits for wavelength-division multiplexing applications," *IEEE J. Sel. Topics Quantum Electron.*, vol. 22, no. 6, pp. 370–378, Dec. 2016.
[2] K. Chen *et al.*, "Experimental demonstration of simultaneous mode and polarization-division multiplexing based on silicon densely packed waveguide array," *Opt. Lett.*, vol. 40, pp. 4655–4658, 2015.
[3] J. M. Hong *et al.*, "Design and fabrication of a significantly shortened multimode interference coupler for polarization splitter application," *IEEE Photon. Technol. Lett.*, vol. 15, no. 1, pp. 72–74, Jan. 2003.
[4] T. Liang and H. Tsang, "Integrated polarization beam splitter in high index contrast silicon-on-insulator waveguides," *IEEE Photon. Technol. Lett.*, vol. 17, no. 2, pp. 393–395, Feb. 2005.
[5] Y. Zhang *et al.*, "High-extinction-ratio silicon polarization beam splitter with tolerance to waveguide width and coupling length variations," *Opt. Exp.*, vol. 24, pp. 6586–6593, 2016.
[6] H. Fukuda, K. Yamada, T. Tsuchizawa, T. Watanabe, H. Shinojima, and S.-I. Itabashi, "Ultrasmall polarization splitter based on silicon wire waveguides," *Opt. Exp.*, vol. 14, pp. 12401–12408, 2006.
[7] F. Zhang, H. Yun, Y. Wang, Z. Lu, L. Chrostowski, and N. A. Jaeger, "Compact broadband polarization beam splitter using a symmetric directional coupler with sinusoidal bends," *Opt. Lett.*, vol. 42, pp. 235–238, 2017.
[8] D. Dai, Z. Wang, and J. E. Bowers, "Ultrashort broadband polarization beam splitter based on an asymmetrical directional coupler," *Opt. Lett.*, vol. 36, pp. 2590–2592, 2011.
[9] J. R. Ong *et al.*, "Broadband silicon polarization beam splitter with a high extinction ratio using a triple-bent-waveguide directional coupler," *Opt. Lett.*, vol. 42, pp. 4450–4453, 2017.

[10] H. Wu, Y. Tan, and D. Dai, "Ultra-broadband high-performance polarizing beam splitter on silicon," *Opt. Exp.*, vol. 25, pp. 6069–6075, 2017.
[11] N. Zhao, C. Qiu, Y. He, Y. Zhang, and Y. Su, "Broadband polarization beam splitter by using cascaded tapered bent directional couplers," *IEEE Photon. J.*, vol. 11, no. 4, Aug. 2019, Art. no. 4900808.
[12] Y. Kim, M. H. Lee, Y. Kim, and K. H. Kim, "High-extinction-ratio directional-coupler-type polarization beam splitter with a bridged silicon wire waveguide," *Opt. Lett.*, vol. 43, pp. 3241–3244, 2018.
[13] C. Errando-Herranz, S. Das, and K. B. Gylfason, "Suspended polarization beam splitter on silicon-on-insulator," *Opt. Exp.*, vol. 26, pp. 2675–2681, 2018.
[14] Y. Tian, J. Qiu, C. Liu, S. Tian, Z. Huang, and J. Wu, "Compact polarization beam splitter with a high extinction ratio over S+ C+ L band," *Opt. Exp.*, vol. 27, pp. 999–1009, 2019.
[15] R. Halir *et al.*, "Ultra-broadband nanophotonic beamsplitter using an anisotropic sub-wavelength metamaterial," *Laser Photon. Rev.*, vol. 10, pp. 1039–1046, 2016.
[16] Y. Wang *et al.*, "Compact broadband directional couplers using subwavelength gratings," *IEEE Photon. J.*, vol. 8, no. 3, Jun. 2016, Art. no. 7101408.
[17] K. Chen, J. Yan, S. He, and L. Liu, "Broadband optical switch for multiple spatial modes based on a silicon densely packed waveguide array," *Opt. Lett.*, vol. 44, pp. 907–910, 2019.
[18] A. Herrero-Bermello, J. M. Luque-González, A. V. Velasco, A. Ortega-Moñux, P. Cheben, and R. Halir, "Design of a broadband polarization splitter based on anisotropy-engineered tilted subwavelength gratings," *IEEE Photon. J.*, vol. 11, no. 3, Jun. 2019, Art. no. 6601508.
[19] Y. Xu and J. Xiao, "Compact and high extinction ratio polarization beam splitter using subwavelength grating couplers," *Opt. Lett.*, vol. 41, pp. 773–776, 2016.
[20] L. Xu *et al.*, "Polarization beam splitter based on MMI coupler with SWG birefringence engineering on SOI," *IEEE Photon. Technol. Lett.*, vol. 30, no. 4, pp. 403–406, Feb. 15, 2018.
[21] H. Xu, D. Dai, and Y. Shi, "Ultra-broadband and ultra-compact on-chip silicon polarization beam splitter by using hetero-anisotropic metamaterials," *Laser Photon. Rev.*, vol. 13, 2019, Art. no. 1800349.
[22] B. Shen, R. Polson, and R. Menon, "Increasing the density of passive photonic-integrated circuits via nanophotonic cloaking," *Nature Commun.*, vol. 7, 2016, Art. no. 13126.
[23] S. Jahani *et al.*, "Controlling evanescent waves using silicon photonic all-dielectric metamaterials for dense integration," *Nature Commun.*, vol. 9, 2018, Art. no. 1893.
[24] S. Jahani and Z. Jacob, "Transparent subdiffraction optics: Nanoscale light confinement without metal," *Optica*, vol. 1, pp. 96–100, 2014.
[25] C. Gu and P. Yeh, "Form birefringence dispersion in periodic layered media," *Opt. Lett.*, vol. 21, pp. 504–506, 1996.
[26] W.-P. Huang, "Coupled-mode theory for optical waveguides: An overview," *J. Opt. Soc. Amer. A*, vol. 11, pp. 963–983, 1994.
[27] J. W. Yoon *et al.*, "Time-asymmetric loop around an exceptional point over the full optical communications band," *Nature*, vol. 562, pp. 86–90, 2018.
[28] H. Morino, T. Maruyama, and K. Iiyama, "Reduction of wavelength dependence of coupling characteristics using si optical waveguide curved directional coupler," *J. Lightw. Technol.*, vol. 32, no. 12, pp. 2188–2192, Jun. 2014.
[29] H. Yun, W. Shi, Y. Wang, L. Chrostowski, and N. A. Jaeger, "2 $\times$ 2 adiabatic 3-db coupler on silicon-on-insulator rib waveguides," *Proc. SPIE Photon. North*, vol. 8915, 2013, Art. no. 89150V.
[30] A. Takagi, K. Jinguji, and M. Kawachi, "Wavelength characteristics of (2 $*$ 2) optical channel-type directional couplers with symmetric or nonsymmetric coupling structures," *J. Lightw. Technol.*, vol. 10, no. 6, pp. 735–746, Jun. 1992.
[31] K. Jinguji, N. Takato, A. Sugita, and M. Kawachi, "Mach-Zehnder interferometer type optical waveguide coupler with wavelength-flattened coupling ratio," *Electron. Lett.*, vol. 26, pp. 1326–1327, 1990.
[32] X. Deng, L. Yan, H. Jiang, W. Pan, B. Luo, and X. Zou, "Polarization-insensitive and broadband optical power splitter with a tunable power splitting ratio," *IEEE Photon. J.*, vol. 9, no. 3, Jun. 2017, Art. no. 4501609.
[33] J. Van Campenhout, W. M. Green, S. Assefa, and Y. A. Vlasov, "Low-power, 2 $\times$ 2 silicon electro-optic switch with 110-nm bandwidth for broadband reconfigurable optical networks," *Opt. Exp.*, vol. 17, pp. 24020–24029, 2009.
[34] J. Van Campenhout, W. M. Green, and Y. A. Vlasov, "Design of a digital, ultra-broadband electro-optic switch for reconfigurable optical networks-on-chip," *Opt. Exp.*, vol. 17, pp. 23793–23808, 2009.
[35] A. Y. Piggott, J. Lu, K. G. Lagoudakis, J. Petykiewicz, T. M. Babinec, and J. Vučković, "Inverse design and demonstration of a compact and broadband on-chip wavelength demultiplexer," *Nature Photon.*, vol. 9, pp. 374–377, 2015.
[36] C. Dory *et al.*, "Inverse-designed diamond photonics," *Nature Commun.*, vol. 10, 2019, Art. no. 3309.
[37] J. Jiang, D. Sell, S. Hoyer, J. Hickey, J. Yang, and J. A. Fan, "Free-form diffractive metagrating design based on generative adversarial networks," *ACS Nano*, vol. 13, pp. 8872–8878, 2019.
[38] Y. Kiarashinejad, S. Abdollahramezani, M. Zandehshahvar, O. Hemmatyar, and A. Adibi, "Deep learning reveals underlying physics of light-matter interactions in nanophotonic devices," *Adv. Theory Simul.*, vol. 2, 2019, Art. no. 1900088.